RSC Advances

PAPER

View Article Online
View Journal | View Issue

Cite this: *RSC Adv.*, 2023, **13**, 9654

Exploring the biomedical competency of gamma-radiation aided hydroxyapatite and its composite fabricated with nano-cellulose and chitosan†

Md. Sahadat Hossain, [a] Md. Aftab Ali Shaikh,*[b] Shirin Akter Jahan,[a] Monika Mahmud, [a] Mashrafi Bin Mobarak, [a] Md. Saifur Rahaman,[d] Md. Najem Uddin [c] and Samina Ahmed *[ac]

Received 22nd January 2023
Accepted 16th March 2023

DOI: 10.1039/d3ra00476g

rsc.li/rsc-advances

The well-known biomaterial Ca-hydroxyapatite (Hap) in its pristine form holds the top ranking position in the field of biomedical research and extensive investigation is continuing across the globe to enhance its competency. Hence, having the intention to introduce superior physiognomies (*e.g.* cytotoxicity, haemocompatibility, and bioactivity coupled with antimicrobial and antioxidant activity) in Hap, in this research work, we exposed Hap to 200 kGy γ-radiation. As a result, γ-radiated Hap exhibited extreme antimicrobial (more than 98%) and moderate (~34%) antioxidant properties. On the other hand, cytotoxicity and haemocompatibility of γ-radiated Hap were in good agreement with the ISO 10993-5 and ISO 10993-4 standards respectively. Since, bone and joint infections as well as degenerative disorders *e.g.* osteoarthritis, osteomyelitis, bone injury, and spinal problems have emerged as serious issues and urge a remedial way out, application of γ-radiated Hap could be a promising solution in this regard.

Introduction

Continuous quests in developing synthetic biomaterials for diverse biomedical applications have remarkably enriched the horizon of bone tissue engineering research. However, the impetus of the researchers working in this area is always tempting them to explore further advancements.[1,2] In biomedical research, the phrase tissue engineering was first introduced in the late 20th century, particularly in 1987.[1] This approach is based on utilizing multidisciplinary strategies in amalgamated form to recover or replace biological tissues. However, the issues commonly associated with bone tissue engineering are bone defect and bone grafting. The former one is considered as one of the communal clinical problems while the latter one is the 2nd most frequent tissue transplantation, placed right after blood transfusion.[3] Indeed, a noticeable amplified volume of bone grafting procedures are required per annum worldwide and consequently, the necessity of developing various bone substitute biomaterials is also ascending. On the other hand, speedy development of bone tissue engineering has tagged it as a promising approach for repairing bone defects and scientists across the globe are working to explore novel versions of biomimetic biomaterials. Hitherto, although numerous biomaterials which are suitable for bone tissue engineering (particularly for regeneration and repair of bone defects) have been reported but calcium hydroxyapatite (Hap) commonly known as apatite occupied the top grade position.[4–9] Its outstanding compositional and structural resemblance with the apatitic phase of bone has appended it as the most preferable biomaterial.[4,10–12] However, it is well established that crystallinity of Hap sets a restriction to its dissolution characteristics and thus relaxed mode degradation of crystalline Hap fails to comply with the growth rate of newly formed bone *in vivo*. Nevertheless, the higher dissolution rate of amorphous Hap is a solution to minimize this shortcoming. Amorphous Hap is very similar to the poorly crystalline structure of bony Hap and its faster dissolution ability promotes the scaffold to bond with the adjacent bone. Consequently, researchers began working on amorphous Hap based polymeric scaffolds for bone tissue regeneration quite a while ago.[13] In contrast, application of high energy irradiation processed Hap in bio-scaffold is comparatively a modern field of research and a few number of studies have explored this area.[9,14–19] Hap treated by ion irradiation shows various enhanced properties *e.g.* surface roughness, wettability, cell adherence and drug-loading/releasing capacity.[19]

[a]*Institute of Glass and Ceramic Research and Testing (IGCRT), Bangladesh Council of Scientific and Industrial Research (BCSIR), Dr Qudrat-i-Khuda Road, Dhanmondi, Dhaka-1205, Bangladesh. E-mail: shanta_samina@yahoo.com*

[b]*Bangladesh Council of Scientific and Industrial Research (BCSIR), Dr Qudrat-i-Khuda Road, Dhanmondi, Dhaka-1205, Bangladesh. E-mail: aftabshaikh@du.ac.bd*

[c]*BCSIR Laboratories, Dhaka, Bangladesh Council of Scientific and Industrial Research (BCSIR), Dr Qudrat-i-Khuda Road, Dhanmondi, Dhaka-1205, Bangladesh*

[d]*Institute of Nuclear Science and Technology, Bangladesh Atomic Energy Commission, Dhaka 1349, Bangladesh*

† Electronic supplementary information (ESI) available. See DOI: https://doi.org/10.1039/d3ra00476g

Researchers have explored that Hap can also be applied as the carrier of radionuclide as cost effective, and feasible technique.[20] Thus, different types of radionuclides can be added to this biomaterial either in sorption mode or direct incorporation methods for the application in diagnostic or therapeutic purposes.[21–23] Then again, availability of research works relating to this area is limited which describes the effects of radionuclides on the inhibition or growth of microbes. However, since gamma (γ) radiation is often used to sterilize biomedical materials and sterilization is imperative for Hap to be used in bone defect, our chosen ion irradiation was confined with gamma. Furthermore, exposure of γ-radiation on Hap imparts structural changes resulting increased activation energy as well.[15]

Recently, we have investigated the crystallographic properties of Hap as a function of gamma radiation doses (20, 30, 60, and 80 kGy).[7] In that paper we explored the effect of γ-radiation dose on the crystallographic parameters of Hap and concluded that when crystallographic distinctions become prerequisite for its effective application, γ-radiation should be considered as a first-rate modifying technique. Concerning the viewpoints, here we further intended to explore the biomedical competency of γ-radiated Hap.

Although the well-established gold standard γ-radiation dose for sterilization of biomedical products is 25–35 kGy,[15] several studies have already been carried out employing different doses of γ-radiation. For instance, Bargh *et al.*[24] applied a wide range of gamma radiation doses (2, 4, 5, 10, 25, and 50 kGy) onto periodontological grafts and observed the extreme changes occurred there. In another study, conducting polymer based biomaterials upon exposure to 75 kGy gamma radiation showed promising results while examined for biomedical applications.[25] Influence of gamma radiation (10, 25, 50, 100, 500, 750 and 1000 kGy) on bone, which is a convenient source of natural Hap was also investigated by Leszek *et al.*[26] Concerning these viewpoints and the results of our previous work,[7] here we have chosen a fairly high dose (200 kGy) of γ-radiation to treat Hap synthesized by wet chemical precipitation method. Biomedical competency of this γ-radiation treated Hap samples were then examined by accomplishing few routine tests, *e.g.* (i) cytotoxicity; (ii) haemocompatibility; and (iii) bioactivity. However, to investigate its suitability as a candidate material to prevent post-surgery infections, antimicrobial and antioxidant performance were evaluated simultaneously.

Materials and methods

Materials

All the chemicals used in this research were analytical grade. Phosphoric acid (H_3PO_4), calcium hydroxide ($Ca(OH)_2$), and NH_4OH were procured from E-Merck Germany and no further purification was required. Deionized (DI) water was used throughout the work.

Synthesis of Hap and expose to gamma radiation

A generalized wet chemical method as described elsewhere[15] was followed to synthesize Hap where the reactants $Ca(OH)_2$ and H_3PO_4 were Ca and P sources respectively. The nucleation of Hap was achieved by upholding several sequential conditions which are: (i) fixing the stoichiometric ratio of Ca/P at 1.67; (ii) adding H_3PO_4 to $Ca(OH)_2$ solution at very slow flow rate (dropwise) ensuring non-stop stirring of the mixture; (iii) adjusting reaction environment at high pH (around 10–11) by adding NH_4OH; (iv) ripening synthesized Hap in mother solution for 24 h. After completing desired seasoning, the synthesized Hap was filtered under vacuum, washed carefully and dried at 105 °C. It was then divided into two shares. One half remained as it is and the other half of synthesized Hap was exposed to gamma radiation. Following the safety and securities provided by the International Atomic Energy Agency (IAEA), gamma irradiation arrangement was set at the Institute of Nuclear Science and Technology, Bangladesh Atomic Energy Commission (BAEC). A ^{60}Co gamma source (90 kCi) was used in this case while the selected dose was 200 kGy. The sample was infolded in a polyethylene bag which was completely airtight. 5 g of the powdered Hap sample was packed down in the bag keeping the thinness as low as possible. The sample bag was then exposed to the radiation and it was rotating around the gamma radiation source throughout the radiation process. Such set up facilitated a consistent exposure of gamma radiation on to the Hap sample. The radiation environment was customized by fixing the emission increment rate at 10 kGy/24 h. The complete course of the radiation was piloted at room temperature but in the dark coupled with the presence of air. Schematic diagram of the experimental procedure is illustrated in Fig. 1.

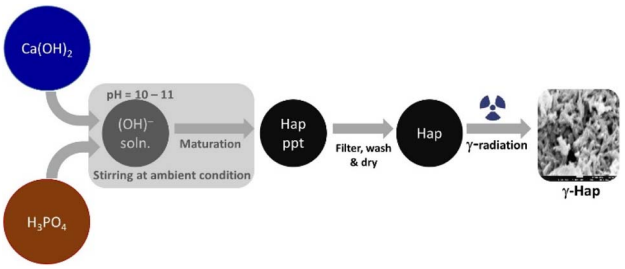

Fig. 1 Synthesis of γ-radiated Hap.

Instrumentation

To characterise the synthesised Hap, we employed X-ray diffractometer (Rigaku SE, Japan). Cu Kα radiation (λ = 1.5406 A) with scan speed 20° min^{-1} facilitated the intensity data to be collected within the chosen scanning range, $2\theta = 10°$–80°. Recorded data were authenticated by matching with the standard JCPDS files. FT-IR and Raman spectroscopic data were collected using FT-IR Prestige 21 (SHIMADZU) equipped with attenuated total reflection (ATR) set-up and Raman spectrometer (HORIBA MacroRAM™ Raman Spectrometer) respectively. To acquire the FT-IR spectra, an average of 30 scans in the range of 400–4000 cm^{-1} coupled with the resolution set up at 4 cm^{-1} were the selected conditions. Contrariwise, facilitating 785 nm wavelength excitation from a diode pumped solid-state laser,

the Raman spectra were recorded in the 3400 cm^{-1} to 100 cm^{-1} region. The output power was regulated at 5 mW. The surface morphology and microstructural features were captured at different magnifications using scanning electron microscope (SEM, Model: Phenom Pro) and field emission scanning electron microscope (FE-SEM, Model: JSM 7610). In case of SEM the accelerating voltages were 10 kV and 15 kV while selected magnification range was 8000×–9000×. On the contrary, applying an accelerating voltage of 5 kV, transmission electron microscope (TEM) images were captured at a magnification of 50 000× using Talos F200X (Thermo Fisher, USA) TEM.

Scaffold fabrication for biomedical competency of γ-Hap

To explore the biomedical competency, together with the γ-Hap we additionally used two organic biomaterials, chitosan (CS) and nano cellulose (CNC) and fabricated the scaffolds. The reason behind using these two biomaterials was to examine how γ-Hap responds singly as well as in composite form. Consequently, three different compositions were selected, *e.g.* (i) 100% γ-Hap; (ii) 70% γ-Hap with 15% CS and 15% CNC; and (iii) 40% γ-Hap with 30% CS and 30% CNC. The materials were characterised by XRD and FT-IR and used either in scaffold form (20 mm diameter and 4 mm thickness) or in powder form depending on the test requirement.

In vitro cytotoxicity assay

Using Trypan Blue Exclusion method,[8,27] cytotoxicity of the composite materials was examined. African Green Monkey Kidney cell (Vero cell) line (CLS 605372, Germany) was cultured for this purpose by adopting an analogous method as referred earlier.[8] Briefly, the Vero cells were cultured in sterile flasks using Dulbecco's Modified Eagles Medium (DMEM) accompanied by other components, *e.g.* (i) fetal bovine serum (FBS, 10% v/v); (ii) 1% penicillin/streptomycin/neomycin (100 U mL^{-1}), (0.1 mg mL^{-1}); and (iii) 25 mM HEPES in 5% (v/v) CO_2. pH was adjusted at 7.4 while the temperature was 37 °C. The cultured cells were treated with three different dosages (25, 50, 100 μg mL^{-1}) of steam sterilized scaffold materials followed by seasoning in trypsin. Each set of experiment was triplicated keeping entire conditions identical and after 72 h of nurturing period the numbers of both unspoiled (viable) and infected (non-viable) cells were computed by an automated cell counter (LUNA-II™, Analytikjena). The cell proliferation/viability was quantified in terms of the percentage of live cells using following equation[27] while significance of the observed results was justified by considering the controlled case experiments. In contrast, to evaluate the cytotoxicity ranking, Table 1 was used.[28]

$$\%\ \text{live cells} = \frac{\text{no. of live cells}}{\text{total amount of cells}} \times 100 \quad (1)$$

Haemolytic assay

Since, haemocompatibility is an indispensable criterion for any biomaterials which will be in direct contact with blood, the fabricated scaffold materials were subjected to haemolytic test following a standard protocol.[29] To accomplish this test, fresh human blood sample was first collected using anti-coagulant heparin and incubated at 37 °C for an hour. The second step involved the preparation of samples where three different concentrations (50, 100, and 200 μg mL^{-1}) of synthesized γ-Hap and the composite materials in phosphate buffer saline (PBS) solution were considered. Hence a total of 9 samples were prepared and each of these samples were subjected to mix with 0.4 mL of incubated blood sample individually. At this stage, all 9 samples were further incubated for another hour. On the other hand, two different controlled media (negative and positive controls) where neither the γ-Hap sample nor the composites were added but incubated with 0.4 mL of blood sample as above. Physiological saline extract and deionized water were the desired negative (*i.e.* 0% haemolysis) and positive (*i.e.* 100% haemolysis) controlled media respectively. However, after going thru all these steps of haemolysis assay, the samples were finally centrifuged at 3000 rpm for 5 minutes. To complete the full package of haemolysis analysis, the absorbance of supernatants were measured at 545 nm (ref. 29 and 30) using UV-Vis spectrophotometer. This measurement aided the calculation of haemoglobin release as an indicator of red blood cell lysis according to the following equation.[29–31]

$$\%\ \text{haemolysis} = \frac{A_{\text{test sample}} - A_{\text{negative control}}}{A_{\text{positive control}} - A_{\text{negative control}}} \times 100 \quad (2)$$

Table 1 Cytotoxicity ranking

Relative growth rate (RGR%) of cell	Cytotoxicity rank
100	0 (*i.e.* no cytotoxicity)
75–99	1 (*i.e.* no cytotoxicity)
50–74	2
25–49	3
1–24	4
0	5

Bioactivity test

Bioactivity of the scaffold material was examined following a previous approach described by S. Sultana *et al.*[8] However, concisely pre-weighed γ-Hap sample was immersed in synthetic body fluid (SBF) and incubated at 37° for two different soaking periods (3 and 7 days). After the completion of each soaking period the change in surface morphology was examined using SEM.

Antimicrobial performance

Antimicrobial activity of γ-radiated Hap was validated following previously published media poisoning technique.[29] The chosen Gram-positive and Gram-negative pathogen bacteria for antibacterial test were *Staphylococcus aureus* (*S. aureus*) and *Escherichia coli* (*E. coli*) respectively while *Aspergillus niger* (*A. niger*) was used to monitor antifungal response. Fixing the ratio of the mixture containing sample and media at one, nutrient

agar media and potato dextrose agar were used to assess antibacterial and antifungal activities. The sterilization process was continued for certain period at a pressure of 15 lbs. Required volume of each sterilized medium was then swabbed individually onto various Petri dishes and using an aseptic glass spreader, each freshly cultured microorganism (maintaining a dilution factor of 15) was dispersed on each plate. The plates were reserved in upturned position followed by a day long and 4 days incubation for bacteria and fungus respectively. Using the following eqn (1), inhibitory effect (η_e) as created by each test material was calculated.[31–33]

$$\eta_e = \frac{C_{\text{colonies at control}} - C_{\text{colonies at sample}}}{C_{\text{colonies at control}}} \times 100\% \quad (3)$$

Antioxidant activity

To evaluate the antioxidant activity of γ-radiated Hap, 2,2-diphenyl-1-picrylhydrazyle (DPPH) free radical scavenging method[34–37] was adapted. The radical solution alone was used as control while the test sample was prepared by adding γ-radiated Hap with DPPH solution. Using the measured absorbance at 515 nm, the ability of γ-radiated Hap to scavenge the DPPH radical was calculated with the aid of the following eqn (2):[35,36]

$$\%\ \text{of DPPH scavenged} = \frac{A_c - A_s}{A_c} \times 100 \quad (4)$$

where A_c and A_s signifies the absorbance of the control and test samples, respectively.

Results and discussion

Characterization of γ-radiated Hap

Crystallographic features are known to be fundamental parameters for Hap while intending for clinical application. Since in this present investigation Hap was exposed to high dose γ-radiation, XRD analysis was carried out to study the crystallographic properties of both as-synthesized and γ-radiated Hap. Particularly, our intension was to examine any change if occurred in the crystallographic properties of Hap due to the effect of gamma radiation. As shown in Fig. 2 is the typical XRD patterns of oven dried and γ-radiated Hap. No apparent changes was witnessed in the crystalline structure of Hap as a result of exposure to γ-radiation. Such observation reflected that the structure of Hap was not upset as a consequence of gamma radiation. This was no doubt a promising outcome. In the diffractograms although all the documented peaks appeared in broad and less intense mode; however, the peaks were in well-agreement with the standard ICDD-PDF no. 9-432 (ref. 33) which is symbolic for hydroxyapatite. The peaks accountable for the planes (002), (102), (211), (202), (310), (222), (213) and (004) were well supported by their respective 2θ positions at 25.92°, 28.83°, 31.97°, 34.10°, 39.52°, 46.68°, 49.57° and 53.31°.[7,33] In both diffractograms, the absence of two noticeable peaks at $2\theta = 32.27°$ and 32.95° (which usually carry the significance of crystalline Hap) ensured the poor crystalline nature of the synthesized Hap. However, as a result of gamma

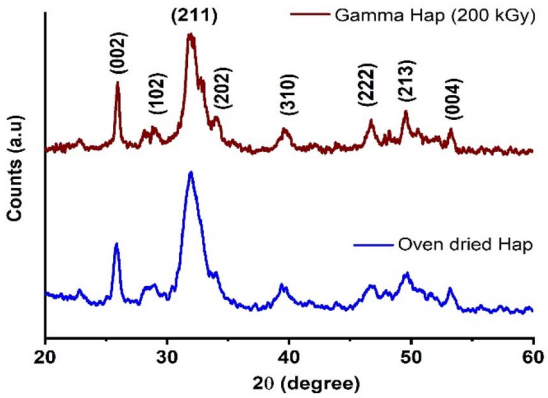

Fig. 2 XRD patterns of oven dried Hap and γ-radiated Hap.

radiation, no phase change occurred although the intensity of (211) plane declined slightly. This observation has also been supplemented by the selected area electron diffraction (SAED) patterns of TEM analysis as described later.

Analogous decrease pattern was also noticed in previous investigation by J. Ramya *et al.* who concluded that this diminution in the intensity of XRD patterns upon γ-irradiation may possibly affects the crystallinity of Hap and favours amorphization.[38] However, since crystallographic properties are considered as an important factor for any biomaterial to be used in bone tissue engineering, next, we evaluated the effect of gamma radiation on the crystallographic properties of Hap. Accordingly, the crystallite size (D_c), crystallinity degree (X_c) and crystallinity index (CI), dislocation density (δ), micro-strain (ε), lattice parameters of γ-Hap were computed using well-established equations[39] and Table 2 represents the corresponding values. Clearly, apart from lattice constants, no significant variation was observed for other parameters considered. The *c*-axis values for both cases although matched with the standard values for Hap (using JCPDS no. 09-432). However, a contraction was observed for *a*-axis of γ-radiated Hap.

FT-IR analysis of the synthesized Hap samples submitted to gamma irradiation was performed for both cases, *i.e.* control group (bare/oven dried Hap) and treated group (γ-radiation exposed Hap). Fig. 3 displays the corresponding FT-IR spectra. The finger print region consists the band positions for PO_4^{3-} groups and their specified signals are: (i) 471 cm^{-1} (ν_2, symmetric bending mode of O–P–O); (ii) 560–605 cm^{-1} (ν_4, asymmetric bending mode of O–P–O); (iii) 960–965 (ν_1, symmetric stretching mode of P–O); and (iv) 1020–1033 cm^{-1} (ν_3, asymmetric stretching mode of P–O).[40] Additional bands at 870–873 cm^{-1} and 1460 cm^{-1} are due to CO_3^{2-} group.[41] Since in XRD pattern we did not notice any representative peak for CO_3^{2-}, hence atmospheric CO_2 could be the source of these CO_3^{2-} signals in FT-IR. However, as a result of γ-radiation the peak for CO_3^{2-} at the later position became indistinguishable and no expressive difference was noticed in case of other absorption bands of finger print region which is fairly similar to the previous observation.[41] Coming back to the functional group region, a considerable effect of γ-radiation was observed.

Table 2 Different parameters of Hap

Parameter	Oven dried Hap	γ-radiated Hap
Crystallite size, nm	5.47	5.47
Degree of crystallinity, %	0.004	0.004
Dislocation density, (10^{15} lines per m^2)	33.38	33.40
Micro-strain, ε	1.31	1.32
Crystallinity index CI_{XRD}	0.19	0.18
Lattice constants of Hap	$a = b = 9.50$ Å, $c = 6.88$ Å, $V = 537.73$ Å	$a = b = 9.35$ Å; $c = 6.86$ Å, $V = 519.37$ Å

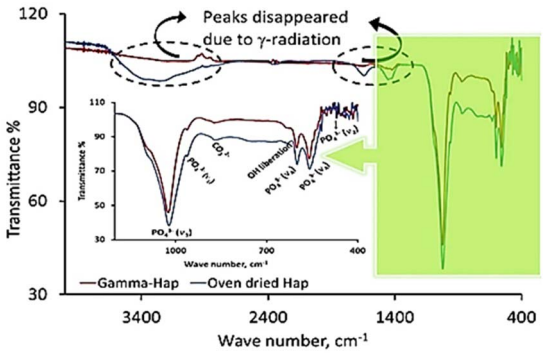

Fig. 3 FT-IR spectra of oven dried and γ-radiated Hap.

The broad band at 3200–3400 cm^{-1} symbolic for the stretching modes of O–H bonds coupled with CO_3^{2-} signal at 1635 cm^{-1} disappeared upon irradiation.

Given in Fig. 4 illustrates the Raman spectra of oven dried and γ-radiated Hap samples. In both cases, the spectra displayed four distinguished vibration bands which are well supportive of the existence of PO_4^{3-} groups in Hap. These bands include: (i) ν_2 bending at 427 cm^{-1}; (ii) ν_4 bending at 589 cm^{-1}; (iii) ν_1 stretching at 962 cm^{-1}; and (iv) ν_3 stretching in the region 1034 cm^{-1}. These findings are on the same wave length with the earlier investigation accomplished by Stammeier *et al.*[42] However, as a result of γ-radiation the Raman band at 962 cm^{-1} in γ-Hap appeared in broad fashion (inset of Fig. 4). Such observation ensures that the amorphous content in γ-Hap increases as a result of γ-radiation.[43]

Surface chemistry and elemental composition of Hap samples were investigated by XPS and the resultant XPS spectra (Fig. 5) discloses the presence of oxygen (O 1s), calcium (Ca 2p), and phosphorus (P 2p) as the major constituents as expected[44,45] and no other elements were detected. Nevertheless, high-energy resolution analysis of individual peaks [inset Fig. 5(a)–(c)] matched with the studies accomplished previously.[33,45] Inset

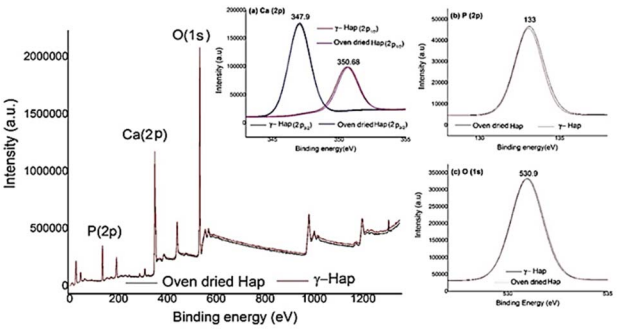

Fig. 5 XPS spectra of oven dried and γ-radiated Hap. Inset (a) exhibits the XPS spectra of Ca 2p having doublet peaks at 347.9 and 350.68 eV and the high resolutions of P 2p and O 1s are presented in the inset of (b) and (c).

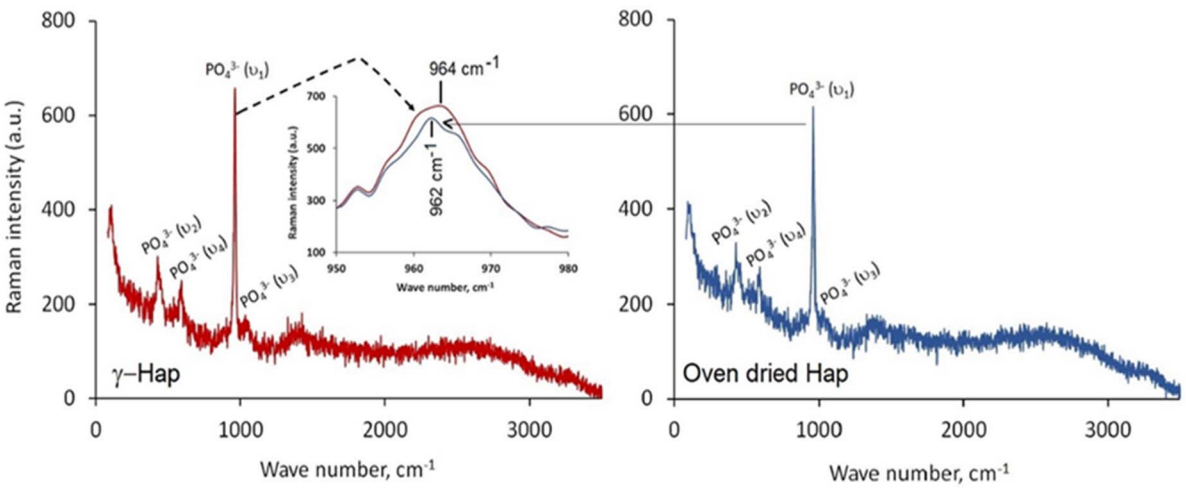

Fig. 4 Raman spectra of oven dried and γ-radiated Hap.

Fig. 5(a) exhibits the XPS spectra of Ca 2p having doublet peaks at 347.9 and 350.68 eV, which resemble to the spin–orbit of $2p_{3/2}$ and $2p_{1/2}$, accordingly. This observation is distinctive for the Ca^{2+} oxidation state in inorganic compounds containing the elements calcium and oxygen.[44] Furthermore, the peak 347.9 eV, credited to Ca bonds distinctive of Hap and to calcium binding with carbonate owing to carbon species adsorbed from atmospheric environment.[45] The presence of atmospheric CO_2 was also supported by FT-IR data. The high resolutions of P 2p and O 1s are presented in the inset Fig. 5(b) and (c). The observed binding energies at 133 eV (for P 2p) and 530.9 eV (for O 1s) signify the presence of P–O bonds of Hap and oxygen bond with phosphate groups together with OH– groups of Hap structure.[45]

The FE-SEM images of without and with γ-radiation processed Hap are appended as ESI data† (Fig. S1a and b) respectively. Hap sample submitted to γ-radiation showed noticeable change in surface morphology. It is quite clear form FE-SEM pictures that before radiation the particles were mostly rod shaped in cluster form. In particular, these nano rods featured like solid bar but in different sizes which were distributed irregularly. Whereas as a result of γ-radiation, Hap particles became needle or spike shaped and less compact and as a consequence, plenty of micro and macro-voids formed which were clearly visible. This is because when high energy gamma radiation was applied the cluster formation was disrupted either through the cleavage of grain boundary or separation of particles and this separation further affected the properties of gamma irradiated Hap. Indeed, gamma irradiation caused a large amount of displacements to be occurred which ultimately hampered the crystallinity of Hap and increased the amorphousness together with increased number of voids. Similar observation was noticed in the TEM images, available as ESI files† (Fig. S2a and b which are representative of oven dried and γ-Hap respectively). Furthermore, lattice fringes were also observed in the TEM images (ESI Fig. S3a and b† representative of oven dried and gamma Hap respectively) while calculated distances between the adjacent lattice fringes agree well for both cases. The rings in the SAED patterns of both samples (ESI Fig. S4a and b†) logged as (002), (102), (211), (310), (222), (321), (323), (004) planes matched with the observed XRD planes of Hap.

Characterization of γ-Hap–CS–CNC

The XRD patterns of (i) 70% γ-Hap with 15% CS and 15% CNC; and (ii) 40% γ-Hap with 30% CS and 30% CNC are given as ESI data† (Fig. S5a). In both the XRD patterns the diffraction angles appeared at 2θ positions 19.30° (region 1) and 22.39° (region 2) consistent with the diffraction pattern of CS and cellulose respectively.[46,47] However, the intensity of these reflections varied significantly with the percentage of the materials. On the other hand, typical XRD reflections favouring the presence of Hap were also notified in the region 3 of the XRD patterns. The presence of these diffraction peaks indicated that the adopted experimental protocol did not disturb the CS, CNC and Hap structures while in combined form. Furthermore, FT-IR spectra (as provided in the ESI data,† Fig. S5b) of γ-Hap–CS–CNC mostly visualized the functional groups responsible for Hap but for other two components characteristic band positions were suppressed probably due to their presence in reduced amount as compared to Hap.

Biomedical competency of gamma radiated Hap and its composites

***In vitro* cytotoxicity assay.** It is well known that the toxic substances usually persuade different damaging effects in cells, *e.g.* membrane destruction or loss; weakening of metabolic activity; and impairment to the genetic material which in turn lead to cell lysis, *i.e.*, cell death. This phenomenon eventually impedes the survival rate of the cell. However, the viability of the cells after being exposed to the three investigated concentrations (25, 50, 100 μg mL^{-1}) of composite materials comprising three selected compositions of γ-Hap, CS and CNC (as mentioned in experimental section) for 72 h are depicted *via* bar charts (Fig. 6). It is clearly evident from the Fig. 6 that all the composite samples exhibit very high percentage (above 92%) of cell viability. According to the ISO 10993-5, a cell viability of 70% is the recommended border for considering any biomaterial as cytocompatible.[48] Hence, the observed cell viability supports the biocompatibility of the prepared composite materials. This high percentage of cell viability then again signifies the RGR% of cell as high corresponding to the cytotoxicity rank one, which also supports the nontoxic characteristic of the prepared composite materials.[28] On the other hand, the corresponding microscopic images of the treated Vero cells along with the controlled conditions are given in Fig. 7. No remarkable change was observed in the cellular apoptotic activity in the scaffolds as a result of incubation under different defined conditions as investigated. This indicates that the survival of the treated Vero cells is in well agreement with that observed in case of no sample application and controlled condition.

Haemolytic assay. The percentage of red blood cells (RBCs) lysis in the presence of the prepared scaffold materials as obtained from the haemolysis assay are summarized in Fig. 8. It is evident from the Fig. 8 that the haemocompatibility of these three sets of scaffold composites are strongly dependent on

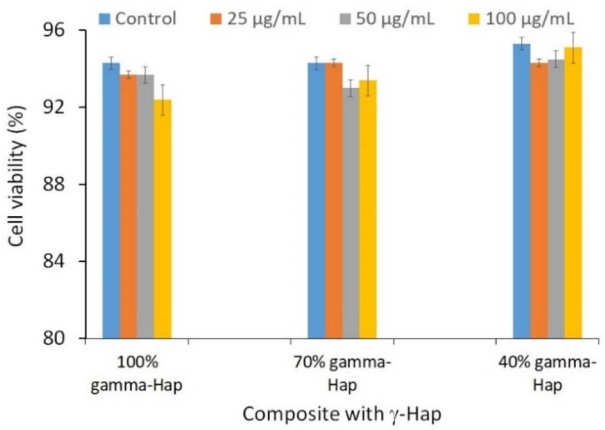

Fig. 6 Cytotoxic effects of γ-Hap and the composite materials (γ-Hap–CS–CNC) having different ratios of Hap.

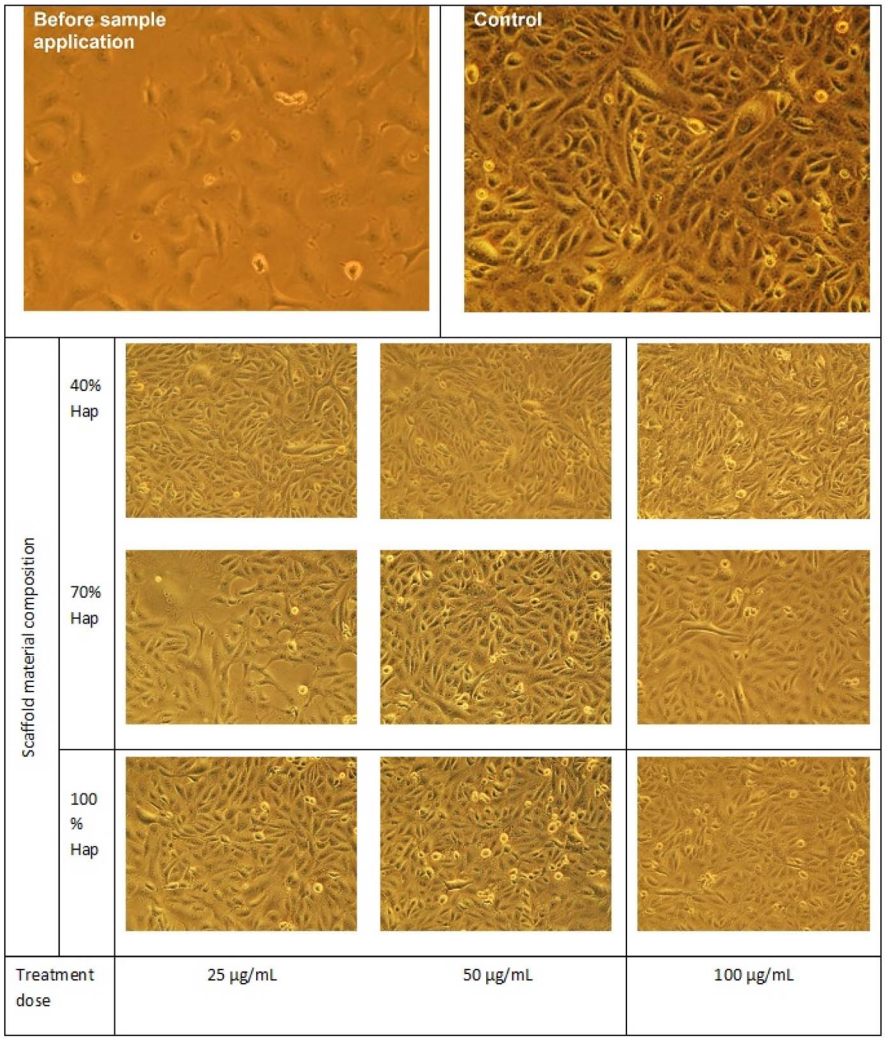

Fig. 7 Microscopic images showing cytotoxic response of γ-radiated Hap and the composite materials (γ-Hap–CS–CNC) having different ratios of Hap.

both the composition of the scaffold and the dosage of biomaterials used to examine haemolysis. The sequences of observed haemolytic properties for both cases are as follows:

Scaffold: 40% γ-Hap < 70% γ-Hap < 100% γ-Hap.

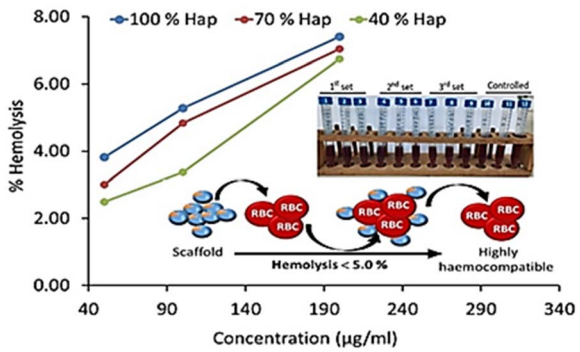

Fig. 8 Haemolysis assay of γ-radiated Hap and the composite materials (γ-Hap–CS–CNC) having different ratios of Hap.

Biomaterial dose: 50 μg mL^{-1} < 100 μg mL^{-1} < 200 μg mL^{-1}.

However, according to the ISO 10993-4 standard[49,50] and ASTM standard[51] three groups of haemolytic ratio are considered: (a) highly haemocompatible (<5% hemolysis); (b) haemocompatible (within 10% haemolysis); and (c) non haemocompatible (>20% hemolysis). The observed haemolysis results for each composite ensured that the lowest dose, 50 μg mL^{-1} concentration of scaffold material exhibited least percentage of haemolysis (within 2.49–3.81%) and thus falls within the category of highly haemocompatible. On the other hand, in case of the composites having 40% and 70% gamma radiated Hap, selected 2nd dose *i.e.* 100 μg mL^{-1} concentration of scaffold material restricted the haemolysis percentage to be 3.37 and 4.83 and thus also qualified as highly haemocompatible. The overall observation as revealed in this study demonstrates the increasing pattern of haemolytic ratio with the increase of dosage which is supported by previous result.[49] Consequently, as a function of 4 times increase in the dose of scaffold material, 2.7–3.0 fold growth in haemolytic ratio was witnessed. The haemolysis percentage as calculated using the

absorbance data representative of highest dose (*i.e.* 200 μg mL^{-1}) of scaffold material of each composite varied within the range 6.7–7.4% and signifies its haemocompatible reaction.[51]

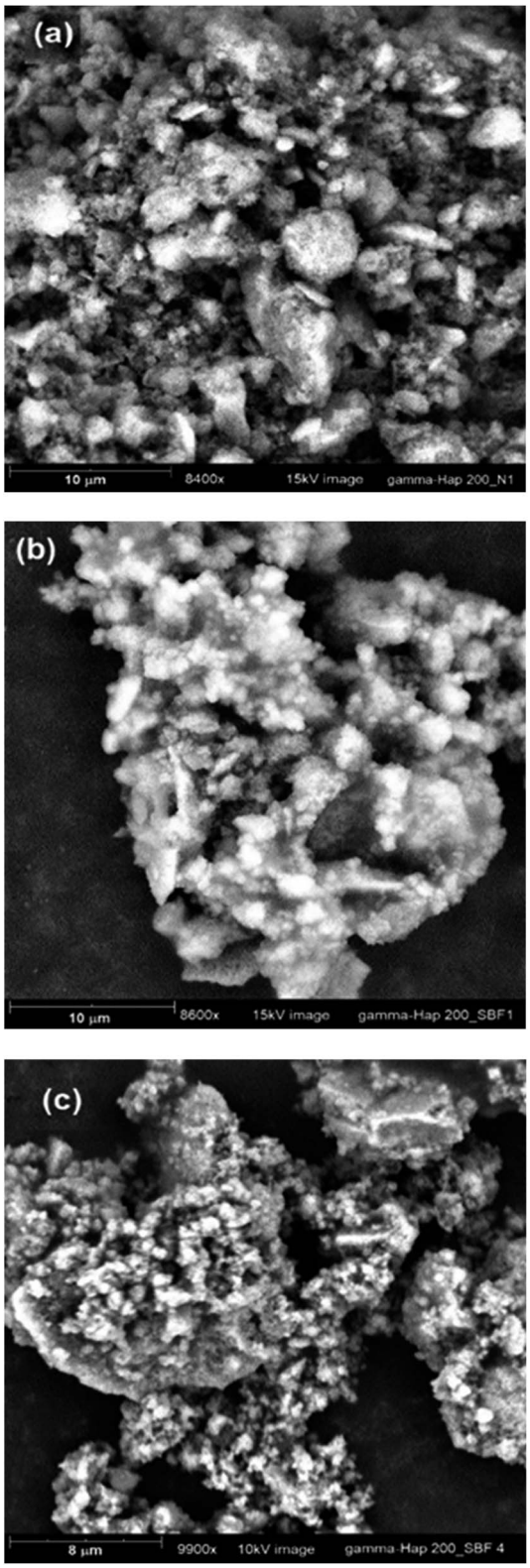

Fig. 9 SEM images of bare γ-Hap (a) and after soaking in SBF; (b) after 3 days; (c) after 7 days.

Bioactivity response. SEM images of bare γ-Hap and after soaking in SBF for 3 and 7 days are given in Fig. 9(a)–(c). The images revealed that as a result of soaking in SBF at 37 °C, an extra layer of apatite started forming on the surface of the sample. However, since the soaking period was not long enough the rate of apatite formation was low.

Simultaneous antimicrobial and antioxidant ability

Antibacterial competency of any biomaterial targeted to be used as implant material is considered as one of the challenging issues to prevent post-surgery infections for both bone and dental grafts. Because, microbial infection unties the implants from the bone.[52] As illustrated in Fig. 10, the antimicrobial and antifungal profile of γ-radiation exposed bare Hap as well as of composites against Gram-positive, Gram-negative pathogen bacteria and fungus are exceptionally promising as compared to the controlled case. Clearly, for all the microorganisms, the colonies growth at control condition are extremely high (3310, 3220 and 3294) and such high rate growth is usually expected for the case of control experiments. On the other hand, the progression of colonies at samples (*i.e.* 100% γ-Hap, 70% γ-Hap and 40% γ-Hap) are significantly low (range 23–550) and varies with the % of Hap. The order of observed antimicrobial and antifungal activities of γ-Hap and its composites are as follows whereas the microscopic images of antimicrobial activity are depicted in ESI Fig S6.†

100% γ-Hap > composite with 70% γ-Hap > composite with γ-40% Hap > control.

Clearly, 100% γ-radiated Hap showed extreme antimicrobial response against the three chosen strains *via* impeding colonies growth by 98.99%, 99.16% and 99.30% (calculated using eqn (3)) for *S. aureus*, *E. coli*, and *A. niger* correspondingly; but the microbial colonies incubated on control surfaces persisted integrally. This is well supported by the observation of Lamkhao *et al.*[53] where the authors also noticed analogous characteristic of microwave irradiated Hap whereas the commercial Hap or simple wet chemical precipitated Hap was non responsive. No antibacterial activity of pure nano Hap was also noticed by Akhavan *et al.*[16] though Sinulingga *et al.*[33] reported insignificant percentage of such activity in natural limestone-derived nano-Hap.

The favourable reason which support these antimicrobial activities is the presence of surface negative charge

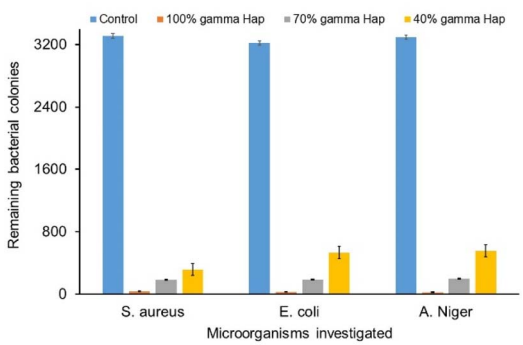

Fig. 10 Antimicrobial activities of γ-Hap containing different compositions.

accompanying the hydrophilic OH functional groups. A repulsive force between the surface and the bacterial cell triggers the antibacterial activity as described earlier.[54] The cell walls of Gram-positive bacteria comprised thick layer of peptidoglycan, a polymer of carbohydrates and charged amino acids, and such a combination subsidized it to be extremely hydrophilic by nature. Moreover, the presence reactive oxygen species (*e.g.* H_2O_2, $OH^{\bullet}$, $O_2^{\bullet-}$) on the surface of Hap also took part in destroying the bacteria.[33,55] On the other hand, the cell walls of Gram-negative bacteria (*E. coli*) are moderately thinner (<10 nm) than those of (20–80 nm) Gram-positive bacteria (*S. aureus*).[56] The composition of the cell walls of *E. coli* include murein, teichoic acids coupled with the wall-attached surface proteins, which expeditiously starts dissolving due to the presence of hydroxyl group of γ-radiated Hap.[57] Nevertheless, in case of *Aspergillus* species, the antifungal activity occurred due to the contribution of phosphate ions of γ-radiated Hap which assists the oxidation of phospholipids of outer cell membrane of the fungus. Thus a diffusion of the outer membranes arose and as a results cytoplasmic outflow led the demise of the pathogen.[57] Using microwave-radiated Hap, a superior antimicrobial activity for both Gram-positive and Gram-negative bacteria was also observed by S. Lamkhao *et al.*[53] The authors, in that research work came up with a conclusion concerning the possible formation of radicals due to microwave irradiation which actively took part to promote antimicrobial activity. Accordingly, here in this present work we further monitored the antioxidant assay *via* DPPH reduction as described in the following section.

Antioxidant activity

The basic approach of DPPH antioxidant process was pioneered by W. Brand-Williams *et al.* in 1995.[34] According to the authors, $DPPH^{\bullet}$ in its radical form, shows the absorbance at 515 nm which then fades out as a result of reduction by an antioxidant (AH) or a radical species ($R^{\bullet}$) and the associated reactions are:

$$DPPH^{\bullet} + AH \rightarrow DPPH - H + A^{\bullet} \quad (5)$$

$$DPPH^{\bullet} + R^{\bullet} \rightarrow DPPH - R \quad (6)$$

Upon the addition of γ-radiated Hap to methanolic solution of DPPH, the distinct violet colour immediately faded away (inset of Fig. 11).[53] This effect was correspondingly noticed in the recorded UV-spectra (Fig. 11) where the absorbance at 515 nm for DPPH drastically reduced for the case of 100% γ-Hap. Such change confirmed the radical scavenging activity of γ-radiated Hap and using eqn (4) it was noted that γ-radiated Hap exhibits about 34% scavenging activity. This observation led to assume the presence of radicals on the surface of γ-radiated Hap and similar consequence was comprehended by Suphatchaya *et al.*[53] which dealt with microwave irradiated Hap. Hence, from the antibacterial, and antioxidant activity data, we conclude that γ-radiated Hap could be a potential candidate for further advancement in biomedical technology particularly in preventing post-surgery infections.

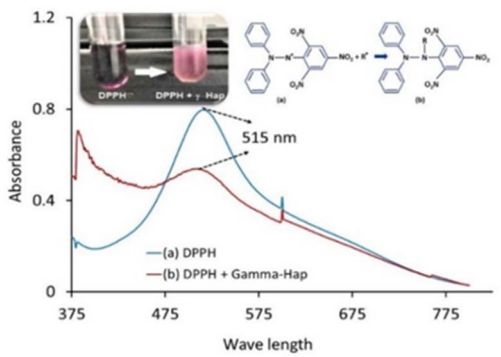

Fig. 11 Colour of DPPH solution changed due to the addition of γ-radiated Hap powder.

Conclusions

We have investigated the performance of γ-radiation exposed Hap as biomimetic scaffold. Benefiting from the advantages of generating free radicals as a result of applying 200 kGy γ-radiation, remarkable antimicrobial efficacy (more than 98% as investigated using three microbial species categorized Gram positive, Gram negative and fungus) was resulted. Besides, γ-Hap also exhibited 34% antioxidant activity and thus retains a unique combination to prevent post-surgery infections. We conclude that the free radicals generated due to high energy ionizing radiation were able to destroy the prokaryotic cell (*e.g.* microbes) but inactive towards the eukaryotic cell (*e.g.* blood cell). Hence, the γ-radiated Hap could be a potential candidate for further advancement in biomedical technology, especially for bio-related applications. Moreover, excellent cyto- and haemo-compatibility were shown by the scaffold materials which ensured that application of gamma radiation did not hampered the usual characteristics.

Ethical statement

All experiments were performed in accordance with the Guidelines of "IGCRT". Experiments were approved by the ethics committee at "BCSIR". Informed consents were obtained from human participants of this study.

Author contributions

M. S. H. and S. A. conceived and designed the experiments; accomplished the data analysis. M. S. H, M. M. and M. B. M. conducted the synthesis and characterization of Hap. M. S. H. and M. N. U. examined the performance of biomimetic scaffolds. M. S. R. accomplished the γ-radiation. S. A. J. provided XPS and XRD. S. A. prepared the manuscript. The research was supervised by M. A. A. S. and S. A.

Conflicts of interest

There are no conflicts to declare.

Acknowledgements

We are gratefully acknowledging the support from IGCRT, BCSIR (R&D approval ref. 39.02.0000.011.14.134.2021/900). Assistance from CARF and BTRI, BCSIR (for providing Raman and FE-SEM facilities) is also appreciated.

References

1 H. Qu, H. Fu, Z. Han and Y. Sun, *RSC Adv.*, 2019, **9**, 26252–26262.
2 M. Filippi, G. Born, M. Chaaban and A. Scherberich, *Front. Bioeng. Biotechnol.*, 2020, **8**, 474.
3 V. Campana, G. Milano, E. Pagano, M. Barba, C. Cicione, G. Salonna, W. Lattanzi and G. Logroscino, *J. Mater. Sci.: Mater. Med.*, 2014, **25**, 2445–2461.
4 M. B. Mobarak, M. S. Hossain, M. Mahmud and S. Ahmed, *Heliyon*, 2021, **7**, e08411.
5 J. Anita Lett, S. Sagadevan, I. Fatimah, M. E. Hoque, Y. Lokanathan, E. Léonard, S. F. Alshahateet, R. Schirhagl and W. C. Oh, *Eur. Polym. J.*, 2021, **148**, 110360.
6 M. Sawada, K. Sridhar, Y. Kanda and S. Yamanaka, *Sci. Rep.*, 2021, **11**, 11546.
7 M. S. Hossain, M. A. A. Shaikh, M. S. Rahaman and S. Ahmed, *Mol. Syst. Des. Eng.*, 2022, **7**, 1239–1248.
8 S. Sultana, M. S. Hossain, M. Mahmud, M. B. Mobarak, M. H. Kabir, N. Sharmin and S. Ahmed, *RSC Adv.*, 2021, **11**, 3686–3694.
9 R. B. Malidarre, I. Akkurt, P. B. Malidarreh and S. Arslankaya, *Radiat. Phys. Chem.*, 2022, **197**, 110208.
10 A. Lotsari, A. K. Rajasekharan, M. Halvarsson and M. Andersson, *Nat. Commun.*, 2018, **9**, 4170.
11 B. Ghiasi, Y. Sefidbakht, S. Mozaffari-Jovin, B. Gharehcheloo, M. Mehrarya, A. Khodadadi, M. Rezaei, S. O. Ranaei Siadat and V. Uskoković, *Drug Dev. Ind. Pharm.*, 2020, **46**, 1035–1062.
12 Z. Chen, X. Wang, J. Luo, B. Zhang, F. Shen, B. Li and J. Yang, *RSC Adv.*, 2022, **12**, 36103–36114.
13 E. K. Cushnie, Y. M. Khan and C. T. Laurencin, *Journal of Biomedical Materials Research Part A*, 2008, **84**, 54–62.
14 R. B. Malidarre, İ. Akkurt, K. Gunoglu and H. Akyildirim, *Int. J. Comput. Sci. Eng.*, 2021, **7**, 143–145.
15 S. Shahabi, F. Najafi, A. Majdabadi, T. Hooshmand, M. Haghbin Nazarpak, B. Karimi and S. M. Fatemi, *Sci. World J.*, 2014, 420616.
16 A. Akhavan, N. Sheikh, F. Khoylou, F. Naimian and E. Ataeivarjovi, *Radiat. Phys. Chem.*, 2014, **98**, 46–50.
17 A. K. Bajpai and H. Bundela, *J. Compos. Mater.*, 2010, **44**, 757–778.
18 M. H. Kim, B. S. Kim, J. Lee, D. Cho, O. H. Kwon and W. H. Park, *Biomater. Res.*, 2017, **21**, 1–9.
19 H. Zhu, D. Guo, H. Zang, D. A. Hanaor, S. Yu, F. Schmidt and K. Xu, *J. Mater. Sci. Technol.*, 2020, **38**, 148–158.
20 S. Chakraborty, T. Das, S. Banerjee, H. D. Sarma and M. Venkatesh, *Nucl. Med. Commun.*, 2006, **27**, 661–668.
21 P. Suchánková, E. Kukleva, E. Nykl, P. Nykl, M. Sakmár, M. Vlk and J. Kozempel, *Nanomaterials*, 2020, **10**, 1632.
22 P. Suchánková, E. Kukleva, K. Štamberg, P. Nykl, M. Vlk and J. Kozempel, *RSC Adv.*, 2020, **10**, 3659–3666.
23 A. V. Severin, M. A. Orlova, E. A. Kushnir and A. V. Egorov, *Russ. Chem. Bull.*, 2022, **71**, 449–456.
24 S. Bargh, M. Silindir-Gunay, A. Y. Ozer, S. Colak, B. Kutlu and R. Nohutcu, *Chem. Phys.*, 2021, **3**, 100046.
25 S. Kim, J.-O. Jeong, S. Lee, J.-S. Park, H.-J. Gwon, S. I. Jeong, J. G. Hardy, Y.-M. Lim and J. Y. Lee, *Sci. Rep.*, 2018, **8**, 1–10.
26 L. Kubisz and M. Po\lomska, *Spectrochim. Acta, Part A*, 2007, **66**, 616–625.
27 N. Khan, F. Afroz, M. N. Begum, S. R. Rony, S. Sharmin, F. Moni, C. M. Hasan, K. Shaha and M. H. Sohrab, *Toxicol. Rep.*, 2018, **5**, 970–976.
28 S. Shanmugam and B. Gopal, *Appl. Surf. Sci.*, 2014, **303**, 277–281.
29 V. P. Padmanabhan, S. N. TSN, S. Sagadevan, M. E. Hoque and R. Kulandaivelu, *New J. Chem.*, 2019, **43**, 18484–18494.
30 J. Prakash, T. S. Kumar, K. S. Venkataprasanna, R. Niranjan, M. Kaushik, D. B. Samal and G. D. Venkatasubbu, *Appl. Surf. Sci.*, 2019, **495**, 143543.
31 C. J. Chi Perera, M. G. Castillo Baas, G. A. Alcocer Lara, S. I. Ramos Borges, A. L. Rodríguez Guzmán, I. Fernández Cervantes and N. Rodríguez Fuentes, *Health Policy Technol.*, 2020, **10**, 423–428.
32 L. Huang, D.-Q. Li, Y.-J. Lin, M. Wei, D. G. Evans and X. Duan, *J. Inorg. Biochem.*, 2005, **99**, 986–993.
33 K. Sinulingga, M. Sirait, N. Siregar and H. Abdullah, *RSC Adv.*, 2021, **11**, 15896–15904.
34 W. Brand-Williams, M.-E. Cuvelier and C. Berset, *LWT-Food Sci. Technol.*, 1995, **28**, 25–30.
35 I. Fatimah, P. W. Citradewi, A. Yahya, B. H. Nugroho, H. Hidayat, G. Purwiandono, S. Sagadevan, S. A. I. S. M. Ghazali and S. Ibrahim, *Mater. Res. Express*, 2021, **8**, 115003.
36 V. Ravichandran, S. Vasanthi, S. Shalini, S. A. A. Shah and R. Harish, *Mater. Lett.*, 2016, **180**, 264–267.
37 A. Nagaraj and S. Samiappan, *Front. Microbiol.*, 2019, **10**, 1757.
38 J. R. Ramya, K. T. Arul, P. Sathiamurthi, K. Asokan and S. N. Kalkura, *Ceram. Int.*, 2016, **42**, 11045–11054.
39 M. Hossain, M. Mahmud, M. B. Mobarak and S. Ahmed, *Chem. Pap.*, 2022, **76**, 1593–1605.
40 A. D. Gomes, A. A. de Oliveira, M. Houmard and E. H. Nunes, *Appl. Radiat. Isot.*, 2021, **174**, 109758.
41 H. Gheisari, E. Karamian and M. Abdellahi, *Ceram. Int.*, 2015, **41**, 5967–5975.
42 J. A. Stammeier, B. Purgstaller, D. Hippler, V. Mavromatis and M. Dietzel, *MethodsX*, 2018, **5**, 1241–1250.
43 M. Di Foggia, U. Corda, E. Plescia, P. Taddei and A. Torreggiani, *J. Mater. Sci.: Mater. Med.*, 2010, **21**, 1789–1797.
44 M. C. Chang and J. Tanaka, *Biomaterials*, 2002, **23**, 3879–3885.
45 G. C. Gomes, F. F. Borghi, R. O. Ospina, E. O. López, F. O. Borges and A. Mello, *Surf. Coat. Technol.*, 2017, **329**, 174–183.

46 R. Kumar, S. Kumari, B. Rai, R. Kumar, S. Sirohi and G. Kumar, *J. Polym. Environ.*, 2020, **28**, 2761–2770.
47 T. A. P. Hai and R. Sugimoto, *RSC Adv.*, 2018, **8**, 7005–7013.
48 ISO, ISO 10993-5:2009 - Biological evaluation of medical devices — Part 5: Tests for in vitro cytotoxicity - Google Search, **https://www.google.com/search?q=ISO+-+ISO+10993-5%3A2009+-+Biological+evaluation+of+medical+devices+%E2%80%94+Part+5%3A+Tests+for+in+vitro+cytotoxicity&oq=ISO+-+ISO+10993-5%3A2009+-+Biological+evaluation+of+medical+devices+%E2%80%94+Part+5%3A+Tests+for+in+vitro+cytotoxicity&aqs=chrome.69i57j69i60l2.1090j0j15&sourceid=chrome&ie=UTF-8**, accessed January 16, 2023.
49 S. Deng, Z. Lin, H. Tang, S. Ullah and Y. Bi, *J. Mater. Res.*, 2019, **34**, 2796–2806.
50 14:00-17:00, ISO 10993-5, **https://www.iso.org/standard/36406.html**, accessed January 16, 2023.
51 V. S. Chandra, K. Elayaraja, K. T. Arul, S. Ferraris, S. Spriano, M. Ferraris, K. Asokan and S. N. Kalkura, *Ceram. Int.*, 2015, **41**, 13153–13163.
52 S. Eraković, A. Janković, C. Ristoscu, L. Duta, N. Serban, A. Visan, I. N. Mihailescu, G. E. Stan, M. Socol and O. Iordache, *Appl. Surf. Sci.*, 2014, **293**, 37–45.
53 S. Lamkhao, M. Phaya, C. Jansakun, N. Chandet, K. Thongkorn, G. Rujijanagul, P. Bangrak and C. Randorn, *Sci. Rep.*, 2019, **9**, 1–9.
54 A. Murakami, T. Arimoto, D. Suzuki, M. Iwai-Yoshida, F. Otsuka, Y. Shibata, T. Igarashi, R. Kamijo and T. Miyazaki, *Nanomedicine*, 2012, **8**, 374–382.
55 C. M. Resmim, M. Dalpasquale, N. I. Vielmo, F. Q. Mariani, J. C. Villalba, F. J. Anaissi, M. M. Caetano and M. M. Tusi, *Prog. Biomater.*, 2019, **8**, 1–9.
56 P. N. Silva-Holguín and S. Y. Reyes-López, *Dose-Response*, 2020, **18**, 1559325820951342.
57 B. Y. Kumar, A. M. Isloor, G. C. Kumar and A. M. Asiri, *Sci. Rep.*, 2019, **9**, 1–13.